Nuclear Medicine and Biology 41 (2014) 217–222

Contents lists available at ScienceDirect

Nuclear Medicine and Biology

journal homepage: www.elsevier.com/locate/nucmedbio

Quantification of dopamine transporter density with [^{18}F]FECNT PET in healthy humans

Jonathon A. Nye [a,*], John R. Votaw [a,b], J. Douglas Bremner [b], Margaret R. Davis [a], Ronald J. Voll [a], Vernon M. Camp [a], Mark M. Goodman [a]

[a] Department of Radiology and Imaging Sciences, Emory University, Atlanta, GA 30329
[b] Department of Psychiatry and Behavioral Sciences, Emory University, Atlanta, GA 30322

ARTICLE INFO

Article history:
Received 9 October 2013
Received in revised form 4 December 2013
Accepted 10 December 2013

Keywords:
Positron emission tomography
Dopamine transporter
Kinetic modeling
FECNT
DAT

ABSTRACT

Introduction: Fluorine-18 labeled 2β-carbomethoxy-3β-(4-chlorophenyl)-8-(2-fluoroethyl)nortropane ([^{18}F]FECNT) binds reversibly to the dopamine transporter (DAT) with high selectivity. [^{18}F]FECNT has been used extensively in the quantification of DAT occupancy in non-human primate brain and can distinguish between Parkinson's and healthy controls in humans. The purpose of this work was to develop a compartment model to characterize the kinetics of [^{18}F]FECNT for quantification of DAT density in healthy human brain.
Methods: Twelve healthy volunteers underwent 180 min dynamic [^{18}F]FECNT PET imaging including sampling of arterial blood. Regional time-activity curves were extracted from the caudate, putamen and midbrain including a reference region placed in the cerebellum. Binding potential, BP_{ND}, was calculated for all regions using kinetic parameters estimated from compartmental and Logan graphical model fits to the time-activity data. Simulations were performed to determine whether the compartment model could reliably fit time-activity data over a range of BP_{ND} values.
Results: The kinetics of [^{18}F]FECNT were well-described by the reversible 2-tissue arterial input and full reference tissue compartment models. Calculated binding potentials in the caudate, putamen and midbrain were in good agreement between the arterial input model, reference tissue model and the Logan graphical model. The distribution volume in the cerebellum did not reach a plateau over the duration of the study, which may be a result of non-specific binding in the cerebellum. Simulations that included non-specific binding show that the reference and arterial input models are able to estimate BP_{ND} for DAT densities well below that observed in normal volunteers.
Conclusion: The kinetics of [^{18}F]FECNT in human brain are well-described by arterial input and reference tissue compartment models. Measured and simulated data show that BP_{ND} calculated with reference tissue model is proportional to BP_{ND} calculated from the arterial input model.

© 2014 Elsevier Inc. All rights reserved.

1. Introduction

Dopamine (DA) plays a crucial role in several central nervous system (CNS) signaling processes including motor, motivational and reward-related functions. Areas of elevated dopamine neuronal density are the striatum, midbrain and olfactory tubercle with lesser amounts in the globus pallidus and subthalamic nucleus [1,2]. The dopamine transporter (DAT) is largely responsible for mediating and terminating signal by the reuptake of the monoamine neurotransmitter DA. Dysregulation of striatal DAT has been observed in neurological diseases such as Parkinson's [3,4] and addiction [5,6]. One study has shown dysregulation of midbrain DAT in adolescents with ADHD [7]. Secondly, altering of brain function by blockade of the DAT has been shown to have a threshold effect, such as in the study of psychostimulant reward pathways of cocaine use [8,9]. These studies have taken advantage of the imaging technique positron emission tomography (PET) to calculate DAT density and occupancy by kinetic analysis of target specific radiopharmaceutical uptake using compartment models.

A large number of PET radiopharmaceuticals have been developed and introduced into humans to map the DAT distribution in the CNS (reviewed in [10]). Of these, determination of DAT density in humans has been performed with carbon-11 labeled 2β-carbomethoxy-3β-(4-iodophenyl)tropane (β-CIT) [11,12], 2β-carbomethoxy-3β-(4-fluorophenyl)tropane (β-CFT) [13,14] and N-(3-iodoprop-2-enyl)-2β-carbomethoxy-3β-(4-methylphenyl)nortropane (PE2I) [15]. Specific binding to the DAT was measured as the uptake ratio between the caudate or putamen and a cerebellum reference regions at the time of pseudo-equilibrium. The cerebellum is assumed to contain negligible DAT binding and the time of equilibrium is typically assumed to occur roughly at the time of peak uptake. Studies with [^{11}C]β-CIT measured uptake ratios of approximately 1.8 at 70 min post-injection [11] but peak uptake did not occur for imaging durations lasting up to 90 min [11,12]. Studies with [^{11}C]β-CFT showed higher uptake ratios of approximately 3 at 90 min post injection but again peak uptake was

* Corresponding author at: Wesley Woods Health Sciences Center, 1841 Clifton Rd. NE, Atlanta, GA 30329. Tel.: +1 404 778 4227; fax: +1 404 712 5689.
E-mail address: jnye@emory.edu (J.A. Nye).

0969-8051/$ – see front matter © 2014 Elsevier Inc. All rights reserved.
http://dx.doi.org/10.1016/j.nucmedbio.2013.12.013

not reached over this measurement duration [12,13]. [^{11}C]PE2I showed the highest specific uptake ratios of 10 with a peak uptake reached quickly at 15 min post-injection [15]. Observing the point of peak uptake and washout over the duration of a PET study is desirable for obtaining reliable estimates of kinetic parameters from compartment models [16]. Quantification of [^{11}C]PE2I was later validated with compartment modeling [17].

Only a few of the above radiotracers have fluorine-18 radiolabeled analogues to take advantage of longer synthesis times, improved specific activity and transportation to facilities without onsite cyclotrons. Four have been used to measuring DAT density in humans including fluorine-18 labeled β-CFT [18], N-3-fluoropropyI-2β-carboxymethoxy-3β-(4-iodophenyl) nortropane (FP-β-CIT) [19], 2β-carbomethoxy-3β-(4-chlorophenyl)-8-(2-fluoroethyl)nortropane (FECNT) [20] and *N*-(3-iodoprop-2-enyl)-2β-carbofluoroethoxy-3β-(4′-methyl-phenyl) nortropane (FE-PE2I) [21]. [^{18} F]β-CFT kinetics are too slow for practical use while [^{18} F]FP-β-CIT, [^{18} F]FECNT and [^{18} F]FE-PE2I measurements can be collected over a reasonable duration that includes peak uptake and washout. The time to peak uptake was fastest for [^{18} F]FE-PE2I compared to [^{18} F]FECNT followed by [^{18} F] FP-β-CIT, which is advantageous for the application of compartment models. Quantification of [^{18} F]FP-β-CIT and [^{18} F]FE-PE2I with compartment models has been published in humans but binding in midbrain was not reported for [^{18} F]FP-β-CIT [22]. Compartment modeling of [^{18} F]FECNT has been employed extensively in non-human primate imaging to evaluated DAT density and drug occupancy [23–25] but it has not been validated in humans.

[^{18} F]FECNT PET imaging in humans can distinguish DAT deficits between Parkinson's patients and normal controls using uptake ratios [20]. Later work by Zoghbi and colleagues showed that metabolism of [^{18} F]FECNT yields a ^{18} F-labeled metabolite that crosses the blood–brain-barrier in rat and monkey brain [26]. These findings suggest the hypothesis that quantification with compartment modeling could be confounded in humans by the presence of a radiolabeled metabolite. In the work by Davis and colleagues [20], arterial blood was collected from normal volunteers but a compartment modeling analysis was not presented. The purpose of this work is to present a compartment model of [^{18} F]FECNT uptake and to examine the possible effect of a radiolabeled metabolite on quantification of DAT density.

2. Methods

2.1. Participants

Seven female and 5 male volunteers (28 ± 8 yrs age) chose to participate following written informed consent. This sample population includes an additional 6 normal volunteers previously unreported in the work published by Davis et al. [20], for a total of 12 participants. All volunteers were judged healthy by absence of past or present psychiatric and neurologic disorders on the basis of medical history, a physical examination and a neurological examination. Volunteers were free of drugs that acted on the CNS system and they were instructed to fast (including caffeine) for 4 hours prior to the PET study. This study was approved by the Emory University Institutional Review Board and Radioactive Drug Research Committee.

2.2. Radiochemistry

[^{18} F]FECNT was synthesized by incorporation of [^{18} F]fluoride into the nortropane precursor 2β-carboxymethoxy-3β-(4-chlorophenyl) nortropane. [^{18} F]FECNT was separated from the reaction products with high performance liquid chromotography. The non-decay corrected yield was approximately 16.5% with radiochemical purity of over 99% [27]. The specific activity of the final product was later measured to be 38 ± 45 GBq/μmol at the end of synthesis [28].

2.3. PET protocol

12 healthy normal volunteers had an arterial catheter placed in the radial artery under local anesthesia for blood sampling and determination of the arterial input function. A venous catheter was placed in the opposite forearm for injection of the radiopharmaceutical. All scans were acquired with an ECAT 921 EXACT scanner (Siemens Medical Solutions/CTI, Knoxville, TN) in 3D mode with an in-plane spatial resolution of 5.9 mm full width at half maximum (FWHM) [29]. Volunteers were placed in the supine position and their heads restrained with a conformable thermoplastic facemask. A 15 min transmission scan was collected using Ge-68 rod sources prior to radiopharmaceutical injection. A 180 minute emission scan was started simultaneously with a 5 min constant bolus infusion of [^{18} F]FECNT using a syringe pump. Emission data were binned into the following framing sequence; 10 x 30 sec, 5 x 1 min, 5 x 10 min, 6 x 20 min. Images were reconstructed with filtered-backprojection and a Hahn pre-filter (cutoff frequency of 1 cycle/cm) giving an isotropic spatial resolution of 8 mm FWHM.

Arterial samples were collected in 1.5 mL aliquots manually from the start of injection every 10 sec for the first 2 min, then every minute up to 10 min, then at 15, 20, 30, 60, 120 and 180 min. Samples were chilled to slow metabolic degradation and centrifuged at high gravity for 20 min to separate the plasma and blood components. The plasma supernatant was extracted in two 200 μL duplicate samples, counted on a NaI Packard Cobra well γ-counter (Perkin-Elmer), and corrected for decay to the radiopharmaceutical injection time. The free fraction of parent in plasma was not measured in these samples.

Seven additional blood samples of 5 mL were collected at 2, 6, 10, 20, 60, 120 and 180 min post injection for determination of the parent fraction in blood. Samples were centrifuged at high gravity for 20 min and the plasma supernatant was mixed with ethyl ether (2 x 1 mL). The ether mix was vortexed for 1 min, centrifuged for 2 min and the ether fraction removed then evaporated to dryness and transferred to counting tubes. The non-ether residue was also counted and together the fraction of parent to total radioactivity in blood was determined. The parent fractions were linearly interpolated to the 1.5 mL sample time points and fitted to a sum of two gaussians and three exponentials by minimizing the residual sums squared. This fit provided the analytical form of the arterial input function for optimization of the compartment modeling routines.

2.4. Image analysis

Intra-frame motion correction was performed using affine transformations and maximization of the mutual information metric [30]. A region of interest (ROI) analysis was used to extract time-activity data from three target regions including the caudate, putamen and midbrain. A reference ROI was also placed in the cerebellum including grey and white matter. No MRI data were collected in this study, therefore a MRI template was warped to each volunteer's data to assist in the ROI delineation of cerebellum. Briefly, the MNI PET template was co-registered to a summed [^{18} F]FECNT image (0 to 180 min) smoothed with a 8 mm Gaussian kernel using the default normalization options in SPM8 [31]. The resultant deformation field was applied to the MNI MRI template thereby transforming the template image into the [^{18} F]FECNT PET native space.

Kinetic analysis of [^{18} F]FECNT uptake began with the general 3-tissue 6-parameter (3 T-6P) compartment model that includes free, non-specific and specific binding compartments [32],

$$\frac{dC_{FT}(t)}{dt} = K_1 C_p(t) + k_4 C_S(t) + k_6 C_{NS}(t) - (k_2 + k_3 + k_5) C_{FT}(t)$$

$$\frac{dC_s(t)}{dt} = k_3 C_{FT}(t) - k_4 C_s(t)$$

$$\frac{dC_{NS}(t)}{dt} = k_5 C_{FT}(t) - k_6 C_{NS}(t)$$

where C_P is the free and protein bound raidoligand in plasma, C_{FT} is the free radioligand in tissue, C_{NS} is the non-specific radioligand binding in tissue, and C_S is the specifically bound radioligand in tissue. The rate constants describing transfer of the radioligand include K_1 (mL/min/g) and k_2 (1/min), representing the unidirectional rate constants corresponding to the influx and efflux of the radioligand across the blood brain barrier. k_3 (1/min) and k_4 (1/min) are proportional to the radioligand association (k_{on}*B_{avail}) and disassociation rates in the specifically bound compartment, where k_{on} is the association rate, B_{avail} is the number of available binding sites, and k_{off} the disassociation rate. k_5 (1/min) and k_6 (1/min) are the corresponding proportional association and disassociation rates of the non-specifically bound compartment.

To improve the reliability of the rate parameter estimation, three assumptions were made in the application of the compartment model. First assumption was that $k_3 > > k_5$ in the high DAT density regions of the caudate, putamen and midbrain, therefore C_{NS} and C_{FT} were combined into a single compartment reducing the model to 2-tissues and 4-parameters (2 T-4P) (K_1, k_2, k_3, k_4). Second assumption was that the cerebellum contained a negligible concentration of the DAT protein. Previously published work has demonstrated no detectable specific binding in the cerebellum of non-human primates following chase studies with specific DAT compounds [27]. Third assumption was that k3 < < k5 in the cerebellum, therefore C_S was eliminated reducing the applied model to 2-tissues and 4-parameters (K_1, k_2, k_5, k_6) representing exchange between C_{FT} and C_{NS}.

In addition, the simplest compartment model case was investigated assuming C_{FT}, C_{NS} and C_S equilibrate quickly leaving a 1-tissue and 2-parameter model (1 T-2P) (K_1, k_2'). Under these assumptions, the parameter k_2' is equal to $k_2/(1 + k_3/k_4)$ in the caudate, putamen and midbrain or $k_2/(1 + k_5/k_6)$ in the cerebellum when compared to the 2 T-4P case. Model parameters were estimated with an iterative nonlinear least squares fit using the Powell method implemented in the Interactive Data Language environment (ITT Visual Solutions, Inc.). Measured data were weighted by their individual frame durations in the chi-squared model figure of merit [24].

A full reference input model (FRTM) was also explored using the 2-tissue 4-parameter (R, k_2, k_3, k_4) model described by Lammertsma et al. [33]. In this model, R represents the ratio of K_1 between the target and reference tissue with the cerebellum assigned as the reference tissue. Lastly, we applied the graphic analysis model for reversible tracers developed by Logan et al. [34] using blood and reference tissue inputs. For the arterial input Logan graphical model, the distribution volume ratio, DVR, was calculated by dividing each of the target region distribution volumes by the cerebellum distribution volume.

The density of available binding sites was estimated by calculating the non-displaceable binding potential (BP_{ND}) from the model fit parameters [35],

$$BP_{ND} = f_{ND} * B_{avail}/K_D = V_T/V_{ND} - 1$$

where f_{ND} is the free parent fraction in the non-displaceable compartment, K_D is the transporter affinity, $V_T = K_1/k_2(1 + k_3/k_4)$ for the 2 T-4P model in the DAT-rich regions and $V_{ND} = K_1/k_2(1 + k_5/k_6)$ for the 2 T-4P model in the reference region. In the 1 T-2P case, k_3 and k_5 are set to zero and these quantities reduce to the ratio of K_1/k_2 in the target and reference regions, respectively. Finally, BP_{ND} was calculated from the reference tissue Logan graphical model by estimating the ratio of the volumes of distribution from the slope of the linear region, BP_{ND} = DVR-1.

The dependence of scan duration on the distribution volume in the caudate and cerebellum were calculated from the arterial input model parameters using time-activity curves of duration 80 min up to 180 min. This analysis was performed to investigate the findings of Zoghbi et al. [26], where it was observed that the distribution volume of the cerebellum increased with scan duration.

2.5. Simulations

Simulated data were generated to assess the effect of non-specific binding in the target regions for a range of BP_{ND} when fitting time-activity curves with a 2 T-4P arterial or reference tissue compartment model. A normal time-activity curve was created for the caudate using the 3 T-6P model, where K_1, k_2, k_3 and k_4 were set to the average rate constants measured in the caudate and k_5 and k_6 to the average rates constants measured in the cerebellum (see Table 1). A second normal time-activity curve was created for the cerebellum using the 2 T-4P model, where K_1, k_2, k_5, k_6 were set to the average rate constants measured in the cerebellum (see Table 1). Noise was added to the time-activity curves using the variance computed between the 2 T-4P model fits and the measured data resulting from the image analysis methods above. These simulations assume that the rate constants describing transfer of [^{18}F]FECNT from C_{FT} to C_{NS} are the same for all regions in the brain.

Beginning with 3 T-6P model simulated time-activity curves for the BP_{ND} we report in our normal volunteers, a hundred time-activity curves were generated for each simulation. A total of eight different BP_{ND} values were simulated where the binding density was decreased from 6 to 0.3 by multiplying k_3 by a half log unit. The simulated time-activity curves were then fit with the 2 T-4P models and the estimated BP_{ND} was plotted against the simulated 3 T-6P model BP_{ND}.

2.6. Statistics

Data are presented as mean ± standard deviation (SD). The Akaike information criterion (AIC) was used to compare fits from the arterial input models (AIC = n*ln(RSS/n) + 2*p, where n = number of data points, RSS = residual sum of squares and p = number model parameters). AIC values were compared by calculating the average difference for each region over all volunteers between the 2 T-4P and 1 T-2P model fits. An AIC difference less than zero indicated a preference for the 2 T-4P model and above zero the 1 T-2P model. Data are reported in the tables as the 95% confidence interval range (CI: mean - 2*SD, mean + 2*SD) and if these ranges excluded zero the model was determined to be statistically preferable to one of the two parameter choices. The Student's t-test was used to determine

Table 1
Kinetic rate constants and calculated volumes of distribution for the 2 T-4P arterial input model.

Region	K_1 (mL/min/g)	k_2 (1/min)	k_3 (1/min)	k_4 (1/min)	V_T (mL/g)	AIC CI range
Caudate	0.269 ± 0.077	0.051 ± 0.021	0.331 ± 0.124	0.058 ± 0.022	38.2 ± 12.1	(−35, 44)
Putamen	0.267 ± 0.050	0.049 ± 0.015	0.304 ± 0.160	0.052 ± 0.023	39.0 ± 11.5	(−18, 21)
Midbrain	0.229 ± 0.055	0.050 ± 0.008	0.005 ± 0.003	0.007 ± 0.004	8.0 ± 2.0	(−120, -1.4)
	K_1 (mL/min/g)	k_2 (1/min)	k_5 (1/min)	k_6 (1/min)		
Cerebellum	0.274 ± 0.051	0.101 ± 0.017	0.005 ± 0.003	0.005 ± 0.002	5.6 ± 0.7	(−136, -6.2)

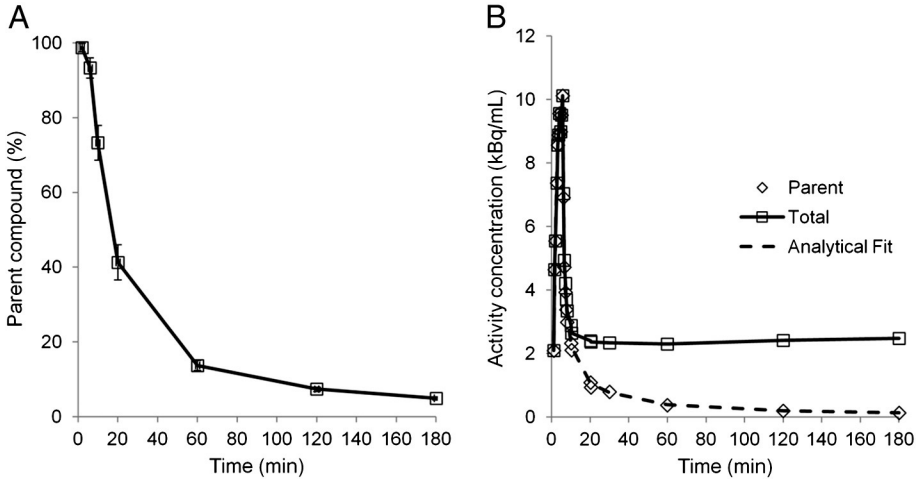

Fig. 1. (A) Percent parent ([^{18} F]FECNT) in arterial plasma post-injection. (B) Representative arterial plasma time-activity curve from a female volunteer injected with 202 MBq [^{18} F]FECNT.

statistical differences between the arterial and reference tissue models parameters. A Bonferonni correction was used to adjust the Type I error, which is reported with the p-value.

3. Results

3.1. PET protocol

The average injected activity was 192 ± 41 MBq. The fraction of [^{18} F]FENCT activity in plasma decreased rapidly from 93% at six minutes post-injection to 7% at 120 min post-injection (Fig. 1A). The total plasma activity was corrected for the fraction of parent using the ether extraction method and plotted over time. The analytical fit to the parent arterial activity concentration is shown with the parent plot (Fig. 1B).

3.2. Image analysis

[^{18} F]FECNT uptake in the caudate and putamen peaked at 50 min post-injection followed by a washout of approximately 0.5%/min (Fig. 2). Uptake in the DAT poor regions of the midbrain and cerebellum peaked earlier at 8 min and decreased rapidly relative to the caudate and putamen.

The arterial input 2 T-4P model described the time-activity curves well but this model was visually indistinguishable from the 1 T-2P in the caudate and putamen (Fig. 2A). Table 1 shows that AIC confidence interval ranges in the caudate and putamen regions were centered roughly about zero suggesting no preference for the 2 T-4P or 1 T-2P models. Furthermore, no statistical difference was found between the distribution volumes calculated between these two models in the caudate or putamen regions (data not shown). For the midbrain, the 2 T-4P model was statistically preferable as indicated from the upper bound of the AIC confidence interval range excluding zero. Similarly, the 2 T-4P model, which included free and non-specific binding, was statistically preferable compared to the 1 T-2P model in the cerebellum.

The Logan graphical model using the arterial input reached linearity in the caudate and midbrain but not in the cerebellum (Fig. 2B and C). Therefore, the measured total distribution volume for the cerebellum was dependent on the start and end point of the linear fit. None of the volunteers showed linearity in the cerebellum as observed in the caudate and midbrain.

BP_{ND} calculated from the model parameters are shown in Table 2 and are in good agreement between the arterial input, reference input

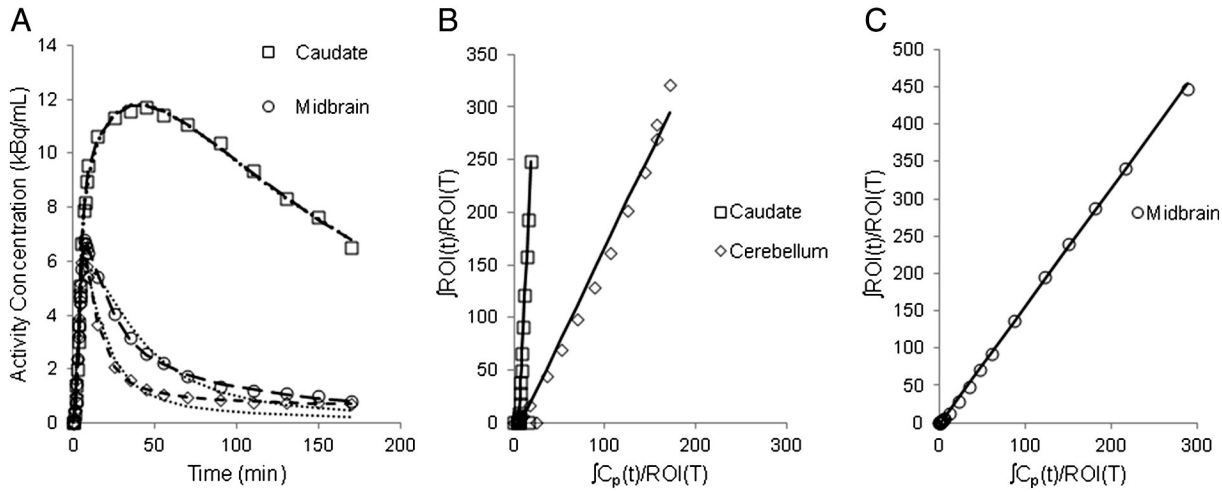

Fig. 2. (A) A representative time-activity curve from a female volunteer injected with 202 MBq of [^{18} F]FECNT. 2 T-4P and 1 T-2P arterial input model fits are shown for the caudate, midbrain and cerebellum. (B) Logan graphical model plots and overlaying linear fits in caudate and cerebellum. (C) Logan graphical model plots and overlaying linear fits in midbrain. The cerebellum does not achieve linearity over the scan duration compared to the DAT-rich structures.

Table 2
Non-displaceable binding potentials, BP_{ND}, for the 2 T-4P arterial input model, FRTM model and Logan graphical method.

Region	Arterial-input model	Reference Model	
	BP_{ND}	BP_{ND} (FRTM)	BP_{ND} (Logan)
Caudate	5.91 ± 2.37	6.10 ± 1.53	5.97 ± 1.44
Putamen	6.02 ± 2.14	6.18 ± 1.26	5.98 ± 1.25
Midbrain	0.44 ± 0.38	0.48 ± 0.14	0.45 ± 0.16

and Logan graphical models. No statistically significant differences were found between the BP_{ND} in any of the regions between the arterial input and reference tissue models. The coefficient of variation (SD/mean x 100%) in the midbrain for the arterial input model was high at 86% compared to the FRTM at 29%.

The total distribution volumes calculated from the 2 T-4P arterial input models for increasing time-activity durations are shown in Fig. 3. The cerebellum distribution volume shows a gradual increase from 4.3 to 5.8 mL/g as the time-activity curve duration increased from 70 to 170 min. Comparatively, the distribution volume in the caudate did not change when the time-activity duration was greater than 100 minutes.

3.3. Simulations

Simulated caudate time-activity curves were generated with the 3 T-6P using the following parameters from Table 1; $K_1 = 0.269$, $k_2 = 0.051$, $k_3 = 0.331$, $k_4 = 0.058$, $k_5 = 0.005$, $k_6 = 0.005$, where k_5 and k_6 are the estimated non-specific compartment transfer parameters from the cerebellum region. Similarly, simulated cerebellum time-activity curves were generated with the 3 T-6P model using the following parameters from Table 1: $K_1 = 0.274$, $k_2 = 0.101$, $k_5 = 0.005$, $k_6 = 0.005$. Fig. 4 shows the results of BP_{ND} estimated from the 2 T-4P fit compared to the simulated data. The addition of the non-specific compartment in the simulations resulted in a positive bias of the reference tissue model BP_{ND} estimate compared to the arterial model BP_{ND} estimate. However both fitting methods show that BP_{ND} estimates from the simulated data are linear down to values of approximately one. At simulated BP_{ND} values of one and lesser, k_5 was on the order of k_3 and the k_3/k_4 estimates converged to the simulated non-specific contant k_5/k_6 values.

4. Discussion

The objective of this work was to develop a kinetic model to quantify the uptake and binding of [^{18} F]FECNT to the dopamine transporter in human brain. In the application of the arterial input models, not all regions were best fit with the same number of compartments and parameters. Based on the AIC, there was no preference between the 2 T-4P and 1 T-2P models for [^{18} F]FECNT in the DAT-rich regions of the caudate and putamen. The lack of a model preference for these regions was also reported for [^{18} F]FP-β-CIT [22]. The slow kinetics of [^{18} F]FP-β-CIT required a time-activity duration of 120 min to show a preference for the 2 T-4P model, whereas shorter durations (<90 min) were best fit with an irreversible 2 T-3P model. The preference for a 2 T-4P model was more clear with [^{18} F]FE-PE2I [21], which has fast kinetics and highly reversible specific binding. In contrast, [^{18} F]FECNT uptake in midbrain showed faster kinetics than the striatum and was best fit with a 2 T-4P model, which was consistent with [^{18} F]FE-PE2I [21]. Midbrain uptake was not reported in the compartment modeling of [^{18} F]FP-β-CIT [22] but has been observed in a small study analyzed with the Logan graphical model [19].

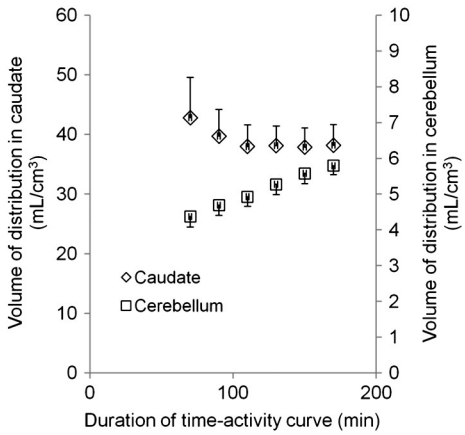

Fig. 3. Average volumes of distribution in the cerebellum and caudate calculated from the 2 T-4P arterial input model as a function of time-activity duration. Error bars represent the standard error.

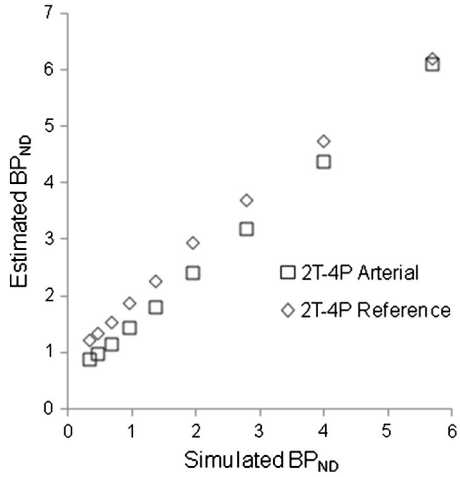

Fig. 4. Simulated BP_{ND} calculated from a 3 T-6P model and the estimated BP_{ND} from the 2 T-4P arterial and reference models.

Application of reference tissue and graphical models are generally favored because they circumvent the need for arterial sampling. Secondly, the presented models assume no confounding radiolabeled metabolites are present in the image data, which is a potential limitation with [^{18} F]FECNT imaging. Comparison of calculated BP_{ND} values for [^{18} F]FECNT between the arterial and reference input models show good agreement in all regions. Overall binding signal was higher compared to that reported for [^{18} F]FP-β-CIT [22] and [^{18} F]FE-PE2I [21], but the coefficient of variance for each region was larger for [^{18} F]FECNT compared to [^{18} F]FE-PE2I. Results from Figs. 2B and 3 show an absence of pseudo-equilibrium and a steady accumulation of signal from 70 to 170 min post-injection in the cerebellum. This observation was not measured in the caudate likely because this change was much smaller than the measurement error. The accumulation of signal in the cerebellum confirms the observations made by Zoghbi et al. [26] and could be explained by accumulation of the radiolabeled metabolite but no direct evidence was available in this work. Other possible explanations may be separate compartments in the grey and white matter in the cerebellum or non-specific binding in the cerebellum and target regions. Separating the grey and white matter regions could not be investigated in this study because volunteer-specific MRI scans were not available for segmentation. However in the presented analysis, a 2-tissue compartment model provided the best fits to the cerebellum time-activity curves suggesting the presence of a non-specific compartment that was not displaceable in earlier non-human primate studies [27].

Our simulations do address the possibility of a non-specific compartment in the cerebellum and caudate regions. As expected, the estimated BP_{ND} is higher than the simulated BP_{ND} due to the

addition of k_5/k_6 in the calculation of V_T. The reference model estimates of BP_{ND} were even higher because the cerebellum was poorly fit and under estimated by a 1 T-2P model. Thus, these simulations suggest that the reference model assumptions do not hold true for quantification of [^{18} F]FECNT with a large non-specific signal. However BP_{ND} is linear over a large range and can be used to distinguish between normal and lower DAT binding.

Although our observations could support the hypothesis of [^{18} F] FECNT radiolabeled metabolite accumulation in the human brain, the model simulations suggest that the possible effect is of minor concern. The potential of the radiolabeled metabolite to confound the [^{18} F] FECNT image data appears to be negligible on quantifying DAT density in normal volunteers using arterial and reference models for time-activity durations of approximately 100 min or longer.

5. Conclusion

The kinetics of [^{18} F]FECNT in human brain are well-described by arterial input and reference tissue compartment models. Quantification of DAT density with these models show good agreement in the caudate, putamen and midbrain of normal volunteers for time-activity durations greater than 100 min. Simulations of non-specific binding in the reference and target regions suggest that estimates of BP_{ND} may be obtained for DAT densities of approximately five times lower than those reported in healthy controls.

Acknowledgments

This research was sponsored by the Office of Health and Environmental Research, U.S. Department of Energy under Grant No. DE-FG02-97ER62637.

References

[1] Ciliax BJ, Heilman C, Demchyshyn LL, Pristupa ZB, Ince E, Hersch SM, et al. The dopamine transporter: immunochemical characterization and localization in brain. J Neurosci 1995;15(3 Pt 1):1714–23.
[2] Coulter CL, Happe HK, Bergman DA, Murrin LC. Localization and quantification of the dopamine transporter: comparison of [3H]WIN 35,428 and [125I]RTI-55. Brain Res 1995;690(2):217–24.
[3] Innis RB, Seibyl JP, Scanley BE, Laruelle M, Abi-Dargham A, Wallace E, et al. Single photon emission computed tomographic imaging demonstrates loss of striatal dopamine transporters in Parkinson disease. Proc Natl Acad Sci U S A 1993;90(24):11965–9.
[4] Seibyl JP, Marek KL, Quinlan D, Sheff K, Zoghbi S, Zea-Ponce Y, et al. Decreased single-photon emission computed tomographic [123I]beta-CIT striatal uptake correlates with symptom severity in Parkinson's disease. Ann Neurol 1995;38(4): 589–98.
[5] Volkow ND, Wang GJ, Fowler JS, Logan J, Hitzemannn R, Gatley SJ, et al. Cocaine uptake is decreased in the brain of detoxified cocaine abusers. Neuropsychopharmacology 1996;14(3):159–68.
[6] Wang G-J, Volkow ND, Fowler JS, Fischman M, Foltin R, Abumrad NN, et al. Cocaine abusers do not show loss of dopamine transporters with age. Life Sci 1997;61(11): 1059–65.
[7] Jucaite A, Fernell E, Halldin C, Forssberg H, Farde L. Reduced midbrain dopamine transporter binding in male adolescents with attention-deficit/hyperactivity disorder: association between striatal dopamine markers and motor hyperactivity. Biol Psychiatry 2005;57(3):229–38.
[8] Volkow ND, Wang GJ, Fischman MW, Foltin RW, Fowler JS, Abumrad NN, et al. Relationship between subjective effects of cocaine and dopamine transporter occupancy. Nature 1997;386(6627):827–30.
[9] Volkow ND, Wang GJ, Fowler JS, Gatley SJ, Logan J, Ding YS, et al. Dopamine transporter occupancies in the human brain induced by therapeutic doses of oral methylphenidate. Am J Psychiatr 1998;155(10):1325–31.
[10] Stehouwer JS, Goodman MM. Fluorine-18 Radiolabeled PET Tracers for Imaging Monoamine Transporters: Dopamine, Serotonin, and Norepinephrine. PET Clin 2009;4(1):101–28.
[11] Laihinen AO, Rinne JO, Nagren KA, Lehikoinen PK, Oikonen VJ, Ruotsalainen UH, et al. PET studies on brain monoamine transporters with carbon-11-beta-CIT in Parkinson's disease. J Nucl Med 1995;36(7):1263–7.
[12] Rinne JO, Laihinen A, Någren K, Ruottinen H, Ruotsawnen U, Rinne UK. PET examination of the monoamine transporter with [11C]β-CIT and [11C]β-CFT in early parkinson's disease. Synapse 1995;21(2):97–103.
[13] Frost JJ, Rosier AJ, Reich SG, Smith JS, Ehlers MD, Snyder SH, et al. Positron emission tomographic imaging of the dopamine transporter with 11C-WIN 35,428 reveals marked declines in mild Parkinson's disease. Ann Neurol 1993;34(3):423–31.
[14] Wong DF, Yung B, Dannals RF, Shaya EK, Ravert HT, Chen CA, et al. In vivo imaging of baboon and human dopamine transporters by positron emission tomography using [11C]WIN 35,428. Synapse 1993;15(2):130–42.
[15] Halldin C, Erixon-Lindroth N, Pauli S, Chou YH, Okubo Y, Karlsson P, et al. [(11)C] PE2I: a highly selective radioligand for PET examination of the dopamine transporter in monkey and human brain. Eur J Nucl Med Mol Imaging 2003;30(9):1220–30.
[16] Laruelle M, Slifstein M, Huang Y. Relationships between radiotracer properties and image quality in molecular imaging of the brain with positron emission tomography. Mol Imaging Biol 2003;5(6):363–75.
[17] Jucaite A, Odano I, Olsson H, Pauli S, Halldin C, Farde L. Quantitative analyses of regional [11C]PE2I binding to the dopamine transporter in the human brain: a PET study. Eur J Nucl Med Mol Imaging 2006;33(6):657–68.
[18] Laakso A, Bergman J, Haaparanta M, Vilkman H, Solin O, Hietala J. [18 F]CFT [(18 F) WIN 35,428], a radioligand to study the dopamine transporter with PET: characterization in human subjects. Synapse 1998;28(3):244–50.
[19] Kazumata K, Dhawan V, Chaly T, Antonini A, Margouleff C, Belakhlef A, et al. Dopamine Transporter Imaging with Fluorine-18-FPCIT and PET. J Nucl Med 1998;39(9):1521–30.
[20] Davis MR, Votaw JR, Bremner JD, Byas-Smith MG, Faber TL, Voll RJ, et al. Initial human PET imaging studies with the dopamine transporter ligand 18 F-FECNT. J Nucl Med 2003;44(6):855–61.
[21] Sasaki T, Ito H, Kimura Y, Arakawa R, Takano H, Seki C, et al. Quantification of Dopamine Transporter in Human Brain Using PET with 18 F-FE-PE2I. J Nucl Med 2012;53(7):1065–73.
[22] Yaqub M, Boellaard R, van Berckel BNM, Ponsen MM, Lubberink M, Windhorst AD, et al. Quantification of dopamine transporter binding using [18 F]FP-[beta]-CIT and positron emission tomography. J Cereb Blood Flow Metab 2006;27(7): 1397–406.
[23] Howell LL, Murnane KS. Nonhuman primate neuroimaging and the neurobiology of psychostimulant addiction. Ann N Y Acad Sci 2008;1141:176–94.
[24] Votaw JR, Howell LL, Martarello L, Hoffman JM, Kilts CD, Lindsey KP, et al. Measurement of dopamine transporter occupancy for multiple injections of cocaine using a single injection of [F-18]FECNT. Synapse 2002;44(4): 203–10.
[25] Masilamoni G, Votaw J, Howell L, Villalba RM, Goodman M, Voll RJ, et al. (18)F-FECNT: validation as PET dopamine transporter ligand in parkinsonism. Exp Neurol 2010;226(2):265–73.
[26] Zoghbi SS, Shetty HU, Ichise M, Fujita M, Imaizumi M, Liow JS, et al. PET imaging of the dopamine transporter with 18 F-FECNT: a polar radiometabolite confounds brain radioligand measurements. J Nucl Med 2006;47(3):520–7.
[27] Goodman MM, Kilts CD, Keil R, Shi B, Martarello L, Xing D, et al. 18 F-labeled FECNT: a selective radioligand for PET imaging of brain dopamine transporters. Nucl Med Biol 2000;27(1):1–12.
[28] Voll RJ, McConathy J, Waldrep MS, Crowe RJ, Goodman MM. Semi-automated preparation of the dopamine transporter ligand [18 F]FECNT for human PET imaging studies. Appl Radiat Isot 2005;63(3):353–61.
[29] Wienhard K, Eriksson L, Grootoonk S, Casey M, Pietrzyk U, Heiss WD. Performance evaluation of the positron scanner ECAT EXACT. J Comput Assist Tomogr 1992;16(5):804–13.
[30] Maes F, Collignon A, Vandermeulen D, Marchal G, Suetens P. Multimodality image registration by maximization of mutual information. IEEE Trans Med Imaging 1997;16(2):187–98.
[31] Ashburner J, Friston KJ. Nonlinear spatial normalization using basis functions. Hum Brain Mapp 1999;7(4):254–66.
[32] Koeppe RA, Frey KA, Mulholland GK, Kilbourn MR, Buck A, Lee KS, et al. [11C] Tropanyl Benzilate-Binding to Muscarinic Cholinergic Receptors: Methodology and Kinetic Modeling Alternatives. J Cereb Blood Flow Metab 1994;14(1): 85–99.
[33] Lammertsma AA, Bench CJ, Hume SP, Osman S, Gunn K, Brooks DJ, et al. Comparison of Methods for Analysis of Clinical [11C]Raclopride Studies. J Cereb Blood Flow Metab 1996;16(1):42–52.
[34] Logan J, Fowler JS, Volkow ND, Wang GJ, Ding YS, Alexoff DL. Distribution volume ratios without blood sampling from graphical analysis of PET data. J Cereb Blood Flow Metab 1996;16(5):834–40.
[35] Innis RB, Cunningham VJ, Delforge J, Fujita M, Gjedde A, Gunn RN, et al. Consensus nomenclature for in vivo imaging of reversibly binding radioligands. J Cereb Blood Flow Metab 2007;27(9):1533–9.